

# Optically-biased Rydberg microwave receiver enabled by hybrid nonlinear interferometry

Sebastian Borówka,<sup>1,2</sup> Mateusz Mazelanik,<sup>1</sup> Wojciech Wasilewski,<sup>1,2</sup> and Michał Parniak<sup>1,2,\*</sup>

<sup>1</sup>*Centre for Quantum Optical Technologies, Centre of New Technologies,  
University of Warsaw, Banacha 2c, 02-097 Warsaw, Poland*

<sup>2</sup>*Faculty of Physics, University of Warsaw, Pasteura 5, 02-093 Warsaw, Poland*

The rapid development in Rydberg-atomic detection of microwave fields has paved the way to a new type of intrinsically calibrated RF measurements. The coupling of Rydberg vapors medium both to microwave and optical fields allows harnessing the merits of all-optical detection, e.g. weak disruption of the measured field and invulnerability to extremely strong fields, owing to the lack of conventional RF antenna in the detector. The trouble with this approach arises, as the greatest sensitivity is exhibited with the use of additional microwave field acting as a local oscillator, and the measurement can no longer be all-optical. Here we propose a different solution, optical-bias detection, that allows truly all-optical operation, while retaining most of the sensitivity. We tackle the issue of uncorrelated laser phase, emerging in this type of detection, by facilitating separate measurement of the phase spectrum in a nonlinear process and using the results in post-processing. We report the sensitivity of  $176 \text{ nV/cm}/\sqrt{\text{Hz}}$  and reliable operation up to  $3.5 \text{ mV/cm}$  of  $13.9 \text{ GHz}$  electric field, while comparing with the state of the art (although not all-optical) method realized in the same setup.

## INTRODUCTION

While the exceptional sensitivity of Rydberg atoms to microwave (MW) fields has been known from atomic beam and cold-atom experiments, only recent advances enabled sensing using hot-atom vapor cell systems. The original approaches to hot-atom sensors were based on the splitting of an electromagnetically induced transparency (EIT) line due to MW-induced Autler-Townes (A-T) effect. This elegant and simple approach allows for a limited sensitivity [1–3] and enables self-calibration based on atomic constants, yet does not yield phase information. Since then, invaluable progress has been made, extending this method to provide phase information and enhance sensing [4–9] or enable applications in communication protocols [10–18], as well as miniaturization of the receivers [19, 20].

The sensitivity metric has been revolutionized by treating the atoms as a MW mixer with optical output [21, 22], effectively constituting a superheterodyne receiver (superhet) [23]. Further developments allowed consecutive enhancements of the method [24–28] and adapting it to specific problems, such as measurements of angle of arrival [29] and polarization [30].

Atomic superhet reception provides an important link to standard radio communication, where superheterodyne detection method is present in all modern receivers. In the end, however, while the readout is optical, the Rydberg-atom receiver still requires a strong MW local oscillator (LO) for operation. In terms of practical applications, this solution is not ideal, as a MW antenna needs to be a part of the receiver, rendering useless some of the advantages of atomic sensors, such as weakly-disruptive

(stealthy) measurement of electric field. [31]

In this paper we present a different type of Rydberg-atom detection, based on optically-biasing ("optical-bias") the mixing process, thus erasing the requirement of a MW LO and making the receiver all-optical. Drawing inspiration from our recent discoveries in MW-to-optical conversion in Rydberg atoms [32], we extend the well-established two-photon Rydberg excitation scheme by the addition of two optical fields in the near-infrared, realising three-photon Rydberg excitation scheme via practically Doppler-free  $5D_{5/2}$  energy level (in rubidium), already explored in some earlier works [33, 34]. Effectively the optical fields play the same role as the MW LO in superhet detection – the optical-bias induces beat modulation in the probe field transmission, and the measurement of its amplitude serves as a MW electrometer. Similar approaches have been presented with the use of two RF fields [35, 36], where several all-optical solutions were proposed as well [36].

The most important challenge arising in this approach is the collective laser phase spectrum, which transfers into the modulation signal. In the superhet detection this issue is mitigated by the addition of phase-stable MW LO, which enables phase stabilization for the optical fields, so long as they are reasonably near atomic two-photon resonance. Similar solutions have been presented in cases of two RF transitions [35, 36], however, it is no longer possible in all-optical scheme. We tackle the problem of laser phase by measuring it in a separate process. To get the laser phase reference we employ a difference frequency generation, using the same laser fields. With real-time correlation performed on an field programmable gate array (FPGA) circuit between measured signal and the reference, we are able to remove the introduced phase fluctuations. This way we render the signal laser-noise-free and achieve performance directly comparable to the superhet detection.

---

\* [mparniak@fuw.edu.pl](mailto:mparniak@fuw.edu.pl)

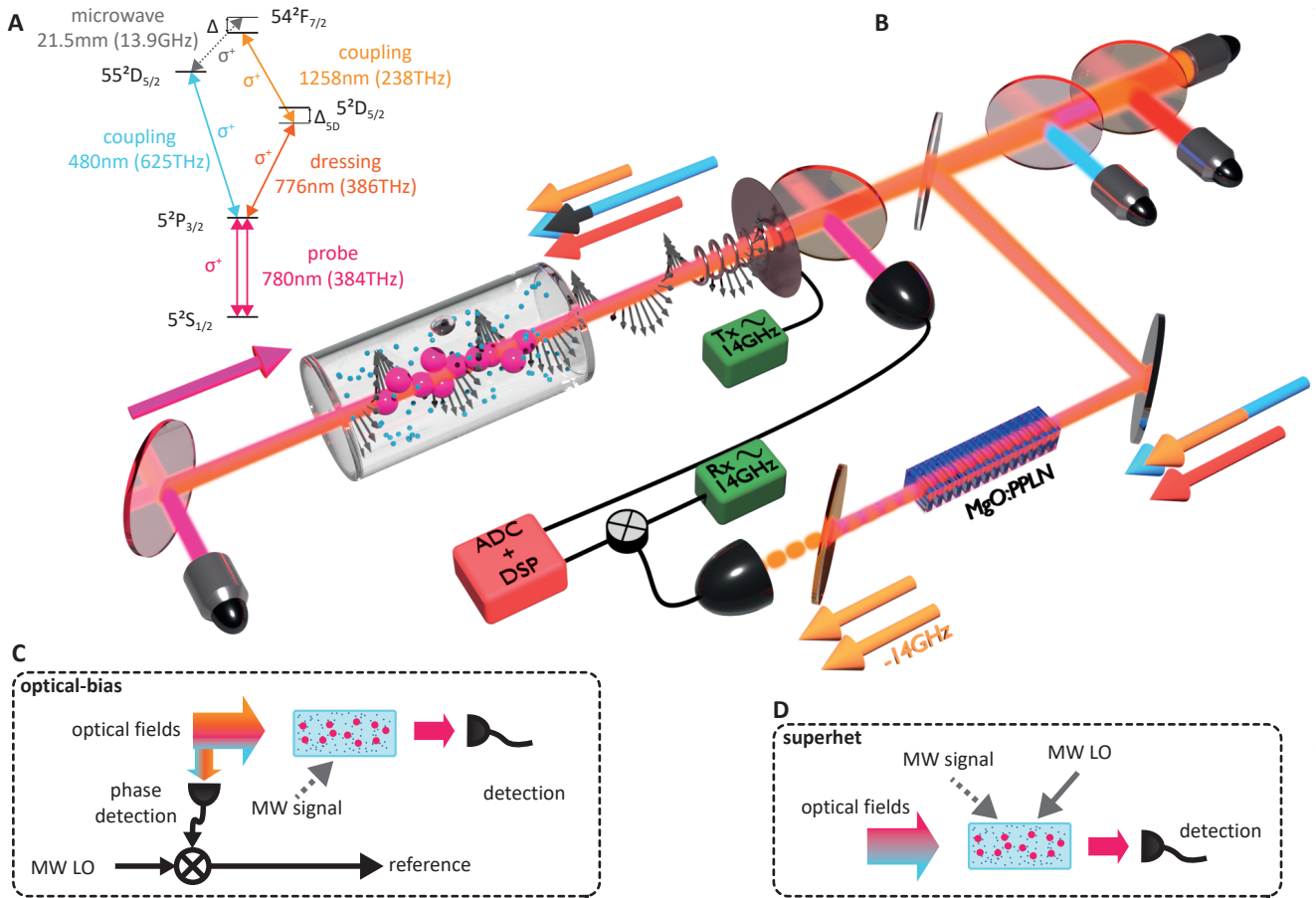


Figure 1. **A**, Energy level structure utilized in the optical-bias detection. Two photon (*probe-coupling*) and three photon (*probe-dressing-coupling*) Rydberg excitation paths are used to access both energy levels connected by the MW transition. The  $\sigma^+$  transitions ensure the largest transition dipole moments. All of the optical fields are atomic resonant, apart from the indicated detuning  $\Delta_{5D} = -1.8$  MHz. The beat modulation in probe transmission is also observed at  $\Delta = 1.8$  MHz due to the detuning of MW field. **B**, Experimental setup of the optical-bias receiver. Three optical (480 nm, 776 nm and 1258 nm) fields are divided into two paths. In the first path they counterpropagate with respect to the 780 nm probe field, enabling partial Doppler effect cancellation. The fields, propagating as Gaussian beams have circular polarizations and are focused to waists of around  $w_0 = 250$   $\mu\text{m}$ , and combined with dichroic mirrors and spectral filters inside  $^{85}\text{Rb}$  vapor cell. The second path leads to frequency generation (DFG) setup for laser phase spectrum detection. The 480 nm and 776 nm fields induce DFG at 1258 nm shifted by the frequency of the detected MW field, as dictated by the conservation of energy. Combined with the non-shifted 1258 nm field used in the detection setup, they induce beat modulation at 13.9 GHz on a photodetector. Then downmixing with LO signal enables the retrieval of laser-noise spectrum shifted to lower frequencies. For measurements, the cell is placed inside a MW absorbing shield with a helical MW antenna acting as a signal source. In the case of superhet detection measured for comparison, the 776 nm and 1258 nm are switched off and MW LO is combined with the signal at the antenna. **C**, Operating principle of a MW optical-bias receiver. An additional measurement of the phase spectrum of optical fields allows the phase compensation. **D**, Operating principle of a MW superhet receiver. The MW LO allows the phase compensation of optical fields.

## RESULTS

*Comparison between superhet and optical-bias MW detection setups* In the superhet detection, pictured schematically in the Fig. 1D, the optical fields, typically probe and coupling beams in counterpropagation enable precise detection of the power of the MW field. Like any fast power detector this setup can be used as a mixer to detect a weak detuned MW signal using a strong res-

onant MW LO. The total MW intensity beats at the frequency of the detuning leading to a modulation in the probe field transmission. The modulation can be then analyzed spectrally to constitute frequency-resolved detection of weak MW electric fields.

On the contrary, in the optical-bias detection, pictured schematically in the Fig. 1C, the weak MW signal is converted to weak optical signal, a sideband of the probe signal, which is subjected to optical heterodyne detection. Thus, the detection stage is conveniently decoupled from

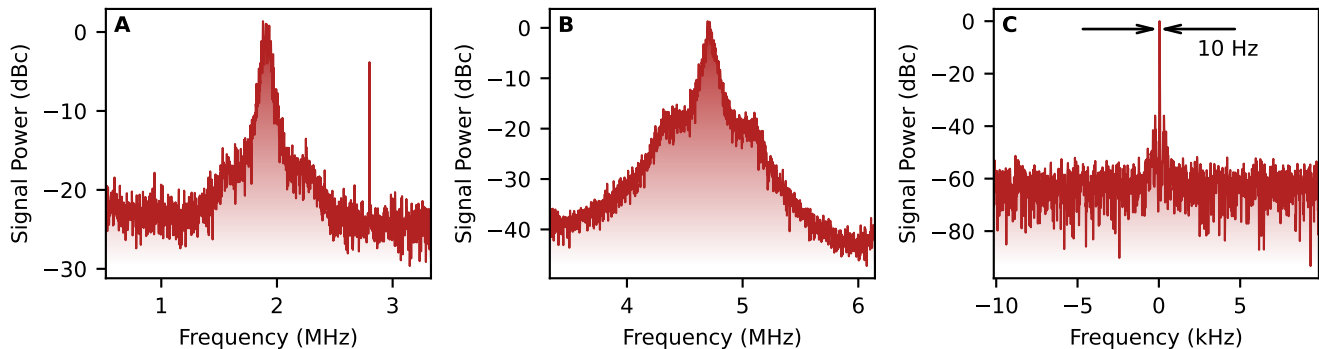


Figure 2. **A**, Spectrum of the probe field modulation obtained in optical-bias detection of  $720 \mu\text{V}/\text{cm}$  MW field. The maximum of the signal is 25 dB above noise level and the spectral width is FWHM. (The visible chime is a small superhet-type signal resulting from cross-talk. It is outside the set detection bandwidth.) **B** Respective spectrum obtained via DFG and beat modulation, as the reference. The maximum of the signal is 41 dB above noise level. **C**, Respective spectrum of the phase-correlated signal. The maximum of the signal is 60 dB above noise level. The spectral width of the signal is Fourier-limited at 10 Hz. The artifact spurs are at  $-38$  dB below the signal.

the volume containing MW field.

Alternative picture involves analyzing MW polarization of the atoms (bias) induced by the laser fields. In this picture, the beating occurs between said polarization and incoming weak MW field. It causes modulation of atomic coherences and modulation of the probe field transmission.

The rubidium energy levels employed in the optical-bias detection are shown in the Fig. 1A. The standard two-photon Rydberg excitation at 780 nm and 480 nm is supplemented with two fields in near-infrared, 776 nm and 1258 nm, both of which are convenient to work with in terms of fiber-based solutions. All of the fields are resonant, apart from the  $\Delta_{5D}$  detuning from the  $5D_{5/2}$  and the beat note detuning,  $\Delta$ . We found the optimal working point when  $\Delta_{5D} = -\Delta$ , as indicated in the Fig. 1C, and set this value to 1.8 MHz.

*Phase reference in superhet and optical-bias detection* Both superhet and optical-bias detection are forms of mixing of the incoming weak MW signal with either supplied MW LO or optical fields performing the role of the LO in optical-bias detection. A mixer detects only the amplitude quadrature of the incoming signal, i.e. only the component in phase with the LO. In case of superhet detection the detection phase is fixed by the reference MW LO. In case of optical-bias detection, the phase information is provided with the polarization (bias) of atoms. This is a result of preparing the atoms with optical fields and therefore every field involved in the process add to the bias effect. There, a relative phase of involved fields  $\phi$  plays a crucial role. In our case, this phase can be expressed as

$$\phi = \phi_{480} - \phi_{1260} - \phi_{776}, \quad (1)$$

where in the subscripts we denote respective optical fields' wavelengths (in nm). Note that the contribution of  $\phi_{780}$  cancels out.

In general, each component of this phase is time-dependent and may be separated into fast-varying (at the optical frequencies) and slow-varying (due to the optical fields phase instabilities). In the interaction picture, via considering rotating wave approximations in relation to each transition between the detuned levels, pictured in the Fig. 1A, only the slow-varying elements remain. These can be then combined into time-dependent slow-varying phase,  $\phi(t)$ . In our approach, instead of minimizing this value (which may be difficult in practice, as one would need to use extremely well stabilized lasers), we decide to register it in a separate process and refer to it in post-processing.

To register the  $\phi(t)$  phase several solutions are possible, including the use of a separate atomic vapor cell with MW LO. In our implementation, we decided to take advantage of an optical nonlinear process. As shown in the Fig. 1C, we realize a difference frequency generation (DFG) between 480 nm and 776 nm field and combine the DFG signal with 1258 nm laser field to detect the beat modulation around 13.9 GHz. The beat modulation is then downconverted to 4.6 MHz and processed electronically on FPGA circuit to yield  $\phi(t)$  measurement in real time.

*Spectral characteristics* An example (detection of  $720 \mu\text{V}/\text{cm}$  MW field) of uncompensated signal in the optical-bias method is presented in the Fig. 2A in relation to noise, which is shot noise of the probe optical field. The spectral FWHM (full width at half maximum) of the signal is 62 kHz. The uncompensated spectral signal shape for monochromatic MW is dictated by collective phase stability of the lasers, thus corresponding to the  $\phi(t)$  phase reference spectrum pictured in the Fig. 2B.

The phase-compensated signal of the example is presented in the Fig. 2C. The measurement duration chosen in this case and in the onward analysis is  $t = 100$  ms, which corresponds to the resolution of 10 Hz. Thus the

noise-compensated signal is Fourier-limited to this resolution. The improvement in the signal in relation to noise, from 25 dB to 60 dB, yielding 35 dB, is consistent with the spectrum-based estimation limit, which is  $(62 \text{ kHz})/(10 \text{ Hz}) = 38 \text{ dB}$ .

The artifact spurs at the level of  $-38 \text{ dB}$  below the signal, are the results of imperfect balancing of MW detection and noise detection setups and can be eliminated with better alignment of the hybrid interferometer.

Note that in the Fig. 2C we present only a part of instantaneously acquired MW spectrum. However in full, we are able to observe real-time measurement of 2 MHz MW bandwidth with 1 Hz resolution (for time base  $t = 1 \text{ s}$ ). To further improve resolution and bandwidth, better electronic solutions need to be employed, and the hybrid interferometer has to be stabilized, e.g. with shortening interferometric arms' lengths of the system or using fiber solutions.

*Dynamic range* With attenuating MW signal we measure the sensitivity of the optical-bias detection method. The results are presented in the Fig. 3, where we facilitate comparison with the superhet method. To achieve adequate comparison, we normalize the signals to respective noise floors, which in both methods are shot noise. In the optical-bias method we find saturation due to energy level shifts at MW field  $3.5 \text{ mV/cm}$ , while the sensitivity reaches  $176 \text{ nV/cm}/\sqrt{\text{Hz}}$ . These results are compared with the superhet method realized in the same setup, where we register the saturation at  $1.84 \text{ mV/cm}$  and the sensitivity of  $87 \text{ nV/cm}/\sqrt{\text{Hz}}$ . Notably, the optical-bias method saturates for larger MW fields, while having lower sensitivity, though the dynamic range is almost equal at 76 dB for  $t = 100 \text{ ms}$  measurement duration.

The behavior of atomic saturation is predicted by the numerical simulation based on the theory model described in the Methods and Materials section. The results comparing the experimental data with the simulated function are presented in the Fig. 3. In this case the shape of the function is predicted with measured parameters and the only free parameter is the constant scaling the overall signal strength.

*Beat modulation transfer* We then perform an experimental analysis of the transfer of beat modulation in probe field detuning domain, once again in the working point of  $720 \mu\text{V/cm}$  MW signal field. We start with the superhet method, where in the probe field absorption, Fig. 4A, we observe widened EIT feature (we found the optimal working point of MW LO to be at only 1.6 MHz Rabi frequency for the beat modulation at 1.8 MHz). Respectively, the modulation transfer dependence is presented in the Fig. 4D, bearing resemblance to the transfer of amplitude modulation of MW field [9].

The optical-bias method exhibits an EIT feature resembling off-resonant A-T splitting due to MW field, although this effect is only due to optical fields, Fig. 4B. The visible EIT outside the  $\pm 10 \text{ MHz}$  range is due to interaction with the sublevels not taking part in the

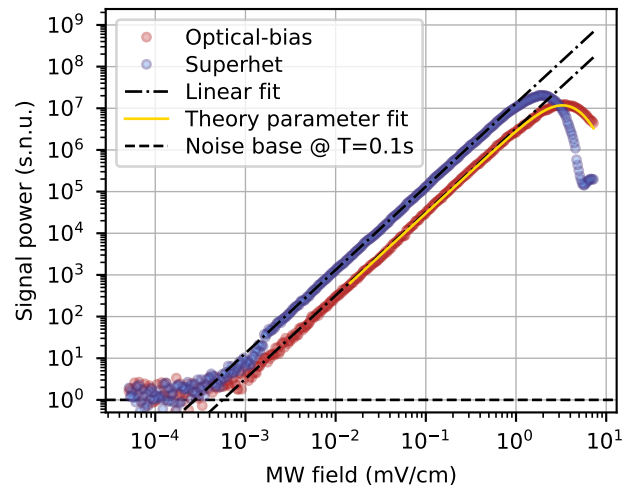


Figure 3. Comparison between results obtained in superhet measurement (blue dots) and optical-bias (red dots). Both results are presented in relation to their respective noise levels (black dashed line), which in both cases is shot noise of the detected probe field transmission. The optical-bias measurement method results in comparable, though smaller sensitivity and overall efficiency. Notably however, it becomes saturated for larger MW fields than the superhet method, thus retaining very similar dynamic range. The results presented here are averaged over  $n = 8$  shots for each point to facilitate better comparison. The yellow solid line represents a theoretical prediction. Notably, the saturation point is predicted accurately and the experimental results differ from the theoretical predictions only in the stronger MW field regime, where the atomic response can no longer be considered instantaneous.

optical-bias detection method, particularly the hyperfine splitting of the  $5P_{3/2}$  and  $5D_{5/2}$  levels. The modulation transfer, Fig. 4E, is similar to the superhet method, when the amplitude of the modulation is considered. However, the phase dependence on probe detuning differs in the direction of transitions.

The results obtained in the numerical simulation based on the theoretical model are shown in the Fig. 4C,F. Both the probe field transmission and the amplitude of modulation are reproduced in terms of shapes in the probe field detuning domain. The difference in the direction of the transition of the phase may be attributed to the interaction with other atomic sublevels visible in the experimental probe transmission, Fig. 4B.

## DISCUSSION

We demonstrated a method of Rydberg atomic detection of MW fields that is both all-optical and sensitive, as shown by the comparison with the standard superhet method. This paves a way to achieving all of the merits of all-optical measurement, i.e. weak disruption of the field and invulnerability to strong interaction, while not com-



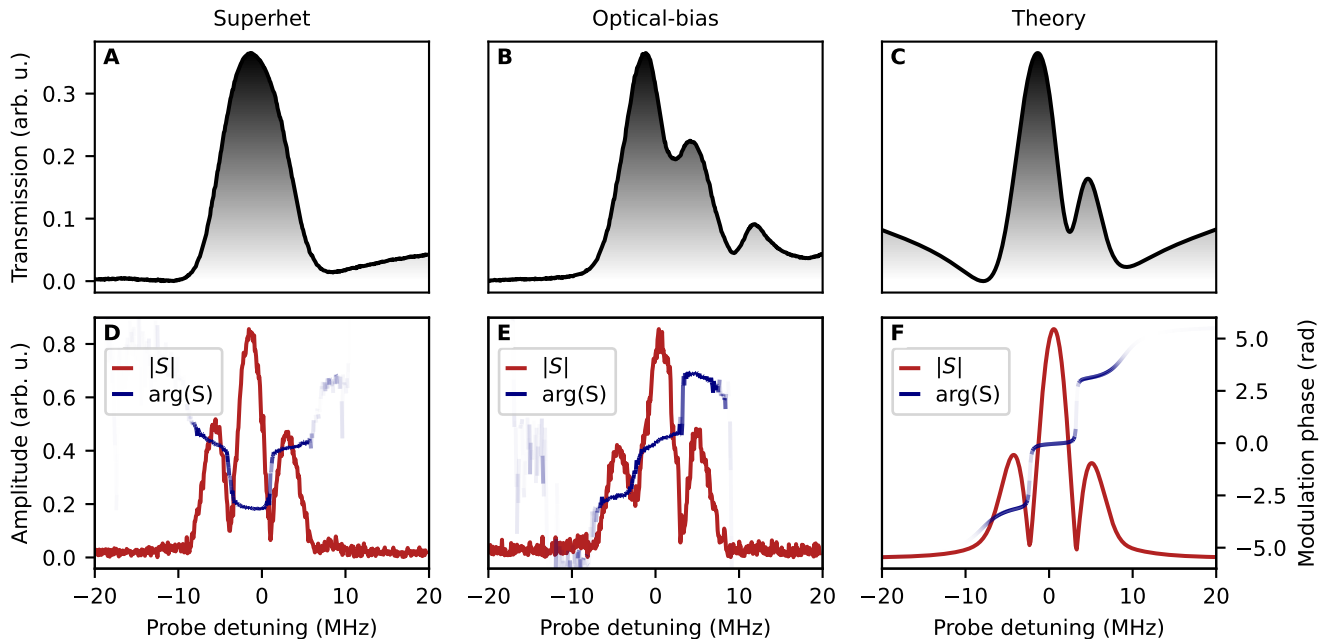


Figure 4. Comparison of EIT effects (upper row) and modulation transfer (lower row), both amplitude  $|S|$  (red lines) and phase  $\arg(S)$  (blue lines) between superhet (left column) and optical-bias (middle column) detection results, and the theoretical prediction for optical-bias (right column) in the domain of probe field detuning. The MW field in all cases is  $720 \mu\text{V}/\text{cm}$ . Notably, despite similarities in the shape of modulation transfer amplitude, the optical-bias method exhibits a different direction of the transition of phase in the demodulated signal than the superhet method. The opacity of blue lines representing phases  $\arg(S)$  is determined by the respective amplitude  $|S|$  to signify measurement uncertainty.

promising on the sensitivity. Furthermore, as the atomic medium interacts with a single MW frequency, it is possible to precisely design a resonant MW cavity around it, which would allow for surpassing the conventional MW receivers [37, 38].

In principle, the demonstrated optical-bias method can be extended to different Rydberg transitions, thus enabling the tunable detection of wide bandwidth of MW and mm-wave frequencies. However, the limitation of the presented realization is the presence of the LO frequency needed to downmix the phase reference signal, which may be difficult for high frequency. This issue can be resolved e.g. with using another vapor cell with LO signal as a reference instead of the DFG mixing demonstrated in this work. Alternatively, one could use an electro-optic modulator with high order sideband modulation to shift one of the laser frequencies in the phase reference setup.

On the other hand, the optical-bias detection method can be massively improved with the use of phase-stable laser fields, e.g. with locking all of the lasers to an optical frequency comb. In this case, if the desired sensitivity and spectral resolution is achieved, the optical-bias would work without the need for additional  $\phi(t)$  phase referencing in a hybrid interferometer.

## METHODS AND MATERIALS

*Theoretical model* To facilitate the comparison with the theoretical predictions, we prepare a numerical simulation based on the following considerations. The atomic state time evolution is described by Gorini–Kossakowski–Sudarshan–Lindblad (GKSL) equation,

$$\partial_t \hat{\rho} = \frac{1}{i\hbar} [\hat{H}, \hat{\rho}] + \mathcal{L}[\hat{\rho}], \quad (2)$$

where  $\hat{H}$  is Hamiltonian and  $\mathcal{L}[\cdot]$  is a superoperator responsible for sources of decoherence, such as spontaneous emission. We consider the steady state solution to the GKSL equation,  $\partial_t \hat{\rho}(t) = 0$ . Atomic numerical data, such as state lifetimes and transition dipole moments, is found via Alkali Rydberg Calculator [39]. To get full agreement with the experiment these operations have to be done for a range of velocity classes present in a room-temperature atomic medium, as well as for a range of laser field power, changing with the radial position in the Gaussian beams.

*Details of optical-bias setup* The MW detection part of the optical-bias setup employed in the experiment is pictured in the Fig. 1C. Four optical Gaussian beams are all focused with Gaussian waists  $w_0 = 250 \mu\text{m}$  inside a rubidium vapor cell. The rubidium is in natural abundance isotope proportion, though only  $^{85}\text{Rb}$  is addressed in this work. The matched optimized Rabi frequencies of

the fields (at the beam centers) are respectively 5.5 MHz, 7.5 MHz, 6.2 MHz and 9.5 MHz for 780 nm, 480 nm, 776 nm and 1258 nm fields. All of the fields have matched circular polarizations. The lasers are stabilized via either cavity transfer locks or optical phase-locked loop to a common reference source (a narrowband fiber laser at 1560 nm, frequency-doubled to 780 nm and referenced to Rb cell with modulation-transfer lock). This results in collective spectral stability of around 62 kHz, as seen in the Fig. 2A,B.

Near the vapor cell acting as a detector, we placed a MW helical antenna acting as a source of weak MW field (and additionally also as a source of MW LO in the superhet measurements facilitated for comparisons). The antenna emits circularly-polarized MW field colinearly with the optical fields. Both the antenna and the vapor cell are placed inside a MW absorbing shield (made from LeaderTech EA-LF500 material), providing protection from MW reflections and on-air noise. The probe laser beam counterpropagates to all the other fields and its power is registered on an avalanche photodiode (Thorlabs APD430A). This detection is shot-noise limited with respect to the probe field power.

*Details of laser phase detection setup* The optical beams 480 nm and 776 nm of respective powers  $\sim 100$  mW and  $\sim 15$  mW are focused and Rayleigh length-matched in a z-cut 30 mm MgO:PPLN crystal with  $5.17 \mu\text{m}$  poling period, at  $\sim 85^\circ\text{C}$ , resulting in 1258 nm DFG signal at  $\sim 25 \mu\text{W}$ . We combine the DFG signal with  $\sim 1$  mW of sampled 1258 nm laser field (which is also propagated through the crystal to reduce the differences in optical paths). Both of 1258 nm fields are then fiber coupled. The beat modulation between them is detected with a fast photodiode (25G SFP28 module for 1310 nm) and serves as an electronic MW phase reference signal.

The phase reference from DFG photodiode is down-mixed with additional MW LO to a frequency of 4.6 MHz convenient for Red Pitaya STEMLab 125-14 ADC/FPGA board used as a measurement tool. The signal is digitized and digitally demodulated, thus providing a complex signal encoding reference phase  $\phi(t)$ . The reference phase is subtracted from the demodulated APD signal yielding a phase corrected signal of optical-bias detection method. Spectra of uncompensated signal, reference phase signal and compensated signal are presented in the Fig. 2.

*Details of the MW setup and calibration* The MW frequency resonant with the  $55^2\text{D}_{5/2} \rightarrow 54^2\text{F}_{7/2}$  transition is measured as  $\omega_0 = 13912.4$  MHz via A-T splitting. The MW signal is then set at  $\omega_0 + \Delta$ , where  $\Delta = 1.8$  MHz. This offset frequency is chosen large enough to avoid any electronic problems at low frequencies and fit within detection bandwidth, resulting in a well resolved sideband on the probe field. The MW signal power is attenu-

ated with a programmable RF attenuator (MiniCircuits RCDAT-18G-63). All MW fields are calibrated using A-T splitting method in the resolvable regime.

In the case of superhet detection, facilitated for comparison, the MW LO is added with a power splitter inserted in the antenna cable. The MW LO is resonant with the atoms and at  $800 \mu\text{V}/\text{cm}$  (1.6 MHz Rabi frequency), which is measured experimentally as optimal in terms of SNR for the set detection parameters, and then combined with the MW signal at the antenna.

All the MW signals are generated with separate LMX2529 PLL frequency synthesizers synchronized to the same clock reference. The signal from APD is measured with the STEMLab 125-14 and digitally demodulated yielding a complex amplitude and phase signal.

## DATA AVAILABILITY

Data underlying the results presented in this paper are available in the Ref. [40].

## CODE AVAILABILITY

The codes used for the numerical simulation and the analysis of experimental data are available from the authors upon request.

## AUTHOR CONTRIBUTIONS

S.B. built the optical, microwave and electronic processing setups. W.W. developed the measurement system firmware and software, assisted by S.B. who programmed the software. S.B. took the measurements and analyzed the data assisted by other authors. S.B., M.M. and M.P. prepared the figures and the manuscript. W.W. developed the theory and numerical simulation assisted by S.B. who facilitated comparison with experiments. M.P. conceived the central idea and led the project assisted by M.M. and W.W.

## ACKNOWLEDGMENTS

We thank K. Banaszek for the generous support. The ‘‘Quantum Optical Technologies’’ (MAB/2018/4) project is carried out within the International Research Agendas programme of the Foundation for Polish Science co-financed by the European Union under the European Regional Development Fund. This research was funded in whole or in part by National Science Centre, Poland grant no. 2021/43/D/ST2/03114.

[1] J. A. Sedlacek, A. Schwettmann, H. Kübler, R. Löw, T. Pfau, and J. P. Shaffer, *Nature Physics* **8**, 819 (2012).

[2] J. A. Sedlacek, A. Schwettmann, H. Kübler, and J. P. Shaffer, *Physical Review Letters* **111**, 063001 (2013).

- [3] H. Fan, S. Kumar, J. Sedlacek, H. Kübler, S. Karimkashi, and J. P. Shaffer, *Journal of Physics B: Atomic, Molecular and Optical Physics* **48**, 202001 (2015).
- [4] S. Kumar, H. Fan, H. Kübler, J. Sheng, and J. P. Shaffer, *Scientific Reports* **7**, 42981 (2017).
- [5] D. A. Anderson, E. G. Paradis, and G. Raithel, *Applied Physics Letters* **113**, 073501 (2018).
- [6] D. H. Meyer, P. D. Kunz, and K. C. Cox, *Physical Review Applied* **15**, 014053 (2021).
- [7] A. Chopinaud and J. Pritchard, *Physical Review Applied* **16**, 024008 (2021).
- [8] X. Liu, F. Jia, H. Zhang, J. Mei, Y. Yu, W. Liang, J. Zhang, F. Xie, and Z. Zhong, *AIP Advances* **11**, 085127 (2021).
- [9] S. Borówka, U. Pylypenko, M. Mazelanik, and M. Parniak, *Applied Optics* **61**, 8806 (2022).
- [10] A. B. Deb and N. Kjærgaard, *Applied Physics Letters* **112**, 211106 (2018).
- [11] D. H. Meyer, K. C. Cox, F. K. Fatemi, and P. D. Kunz, *Applied Physics Letters* **112**, 211108 (2018).
- [12] K. C. Cox, D. H. Meyer, F. K. Fatemi, and P. D. Kunz, *Physical Review Letters* **121**, 110502 (2018).
- [13] Z. Song, H. Liu, X. Liu, W. Zhang, H. Zou, J. Zhang, and J. Qu, *Optics Express* **27**, 8848 (2019).
- [14] C. L. Holloway, M. T. Simons, J. A. Gordon, and D. Novotny, *IEEE Antennas and Wireless Propagation Letters* **18**, 1853 (2019).
- [15] Y. Jiao, X. Han, J. Fan, G. Raithel, J. Zhao, and S. Jia, *Applied Physics Express* **12**, 126002 (2019).
- [16] D. A. Anderson, R. E. Sapiro, and G. Raithel, *IEEE Transactions on Antennas and Propagation* **69**, 2455 (2021).
- [17] J. S. Otto, M. K. Hunter, N. Kjærgaard, and A. B. Deb, *Journal of Applied Physics* **129**, 154503 (2021).
- [18] P. K. Elgee, J. C. Hill, K.-J. E. LeBlanc, G. D. Ko, P. D. Kunz, D. H. Meyer, and K. C. Cox, *Applied Physics Letters* **123**, 084001 (2023).
- [19] M. T. Simons, J. A. Gordon, and C. L. Holloway, *Applied Optics* **57**, 6456 (2018).
- [20] M. T. Simons, A. H. Haddab, J. A. Gordon, D. Novotny, and C. L. Holloway, *IEEE Access* **7**, 164975 (2019).
- [21] M. T. Simons, A. H. Haddab, J. A. Gordon, and C. L. Holloway, *Applied Physics Letters* **114**, 114101 (2019).
- [22] J. A. Gordon, M. T. Simons, A. H. Haddab, and C. L. Holloway, *AIP Advances* **9**, 045030 (2019).
- [23] M. Jing, Y. Hu, J. Ma, H. Zhang, L. Zhang, L. Xiao, and S. Jia, *Nature Physics* **16**, 911 (2020).
- [24] F.-D. Jia, H.-Y. Zhang, X.-B. Liu, J. Mei, Y.-H. Yu, Z.-Q. Lin, H.-Y. Dong, Y. Liu, J. Zhang, F. Xie, and Z.-P. Zhong, *Journal of Physics B: Atomic, Molecular and Optical Physics* **54**, 165501 (2021).
- [25] N. Prajapati, A. K. Robinson, S. Berweger, M. T. Simons, A. B. Artusio-Glimpse, and C. L. Holloway, *Applied Physics Letters* **119**, 214001 (2021).
- [26] H. Li, J. Hu, J. Bai, M. Shi, Y. Jiao, J. Zhao, and S. Jia, *Optics Express* **30**, 13522 (2022).
- [27] J. Hu, H. Li, R. Song, J. Bai, Y. Jiao, J. Zhao, and S. Jia, *Applied Physics Letters* **121**, 014002 (2022).
- [28] M. Cai, S. You, S. Zhang, Z. Xu, and H. Liu, *Applied Physics Letters* **122**, 161103 (2023).
- [29] A. K. Robinson, N. Prajapati, D. Senic, M. T. Simons, and C. L. Holloway, *Applied Physics Letters* **118**, 114001 (2021).
- [30] Y. Wang, F. Jia, J. Hao, Y. Cui, F. Zhou, X. Liu, J. Mei, Y. Yu, Y. Liu, J. Zhang, F. Xie, and Z. Zhong, *Optics Express* **31**, 10449 (2023).
- [31] J. Yuan, W. Yang, M. Jing, H. Zhang, Y. Jiao, W. Li, L. Zhang, L. Xiao, and S. Jia, *Reports on Progress in Physics* **86**, 106001 (2023).
- [32] S. Borówka, U. Pylypenko, M. Mazelanik, and M. Parniak, *Continuous wideband microwave-to-optical converter based on room-temperature rydberg atoms* (2023).
- [33] N. Thaicharoen, K. R. Moore, D. A. Anderson, R. C. Powel, E. Peterson, and G. Raithel, *Physical Review A* **100**, 063427 (2019).
- [34] W. Li, J. Du, M. Lam, and W. Li, *Optics Letters* **47**, 4399 (2022).
- [35] D. Anderson, R. Sapiro, L. Gonçalves, R. Cardman, and G. Raithel, *Physical Review Applied* **17**, 044020 (2022).
- [36] S. Berweger, A. B. Artusio-Glimpse, A. P. Rotunno, N. Prajapati, J. D. Christesen, K. R. Moore, M. T. Simons, and C. L. Holloway, *Physical Review Applied* **20**, 054009 (2023).
- [37] G. Santamaria-Botello, S. Verploegh, E. Bottomley, and Z. Popovic, *Comparison of noise temperature of rydberg-atom and electronic microwave receivers* (2022).
- [38] G. Sandidge, G. S. Botello, and Z. Popović, in *2023 IEEE/MTT-S International Microwave Symposium - IMS 2023* (IEEE, 2023).
- [39] N. Šibalić, J. Pritchard, C. Adams, and K. Weatherill, *Computer Physics Communications* **220**, 319–331 (2017).
- [40] S. Borówka, M. Mazelanik, W. Wasilewski, and M. Parniak, *Replication data for: Optically-biased rydberg microwave receiver enabled by hybrid nonlinear interferometry*, Harvard Dataverse (2024).